Planform selection in two-layer Bénard-Marangoni convection

A. Engel[1,*] and J. B. Swift[2]
[1]*Institut für Theoretische Physik, Otto-von-Guericke Universität, Postfach 4120, D-39016 Magdeburg, Germany*
[2]*Department of Physics and Center for Nonlinear Dynamics, University of Texas at Austin, Austin, Texas 78712*
(Received 2 March 2000)

Bénard-Marangoni convection in a system of two superimposed liquids is investigated theoretically. Extending previous studies, the complete hydrodynamics of both layers is treated and buoyancy is consistently taken into account. The planform selection problem between rolls, squares, and hexagons is investigated by explicitly calculating the coefficients of an appropriate amplitude equation from the parameters of the fluids. The results are compared with recent experiments on two-layer systems in which squares at onset have been reported.

PACS number(s): 47.20.Dr, 47.20.Bp, 47.54.+r, 68.10.−m

I. INTRODUCTION

The hexagonal convection cells discovered by Bénard in his famous experiments on thin oil layers heated from below [1] have become the trademark of pattern formation in hydrodynamic systems driven slightly out of equilibrium (see, e.g., [2]). The 100 years of research devoted to this system have revealed several important insights but also witnessed several misconceptions. Rayleigh's original theoretical description [3] focusing on buoyancy-driven convection, although indicating a possible instability mechanism, failed to produce a threshold compatible with experiment. Not until 40 years later was it realized that the temperature dependence of the surface tension is the crucial driving force in thin layers [4]. The corresponding linear stability analysis [5] gave stability thresholds consistent with the experimental findings; moreover, a subsequent weakly nonlinear analysis [6,7] produced theoretical support for a subcritical transition to a hexagonal flow pattern [8].

Quite naturally the first theoretical investigations were performed using simplified models of the experimental situation. The initial assumption of a flat surface of the liquid was soon relaxed by Scriven and Sternling [9] and Smith [10], who were able to show that surface deflections give rise to an additional instability appearing at very long wavelengths. It was only very recently that this instability was unambiguously demonstrated in an experiment [11], where it manifests itself as a distortion of the layer thickness with a characteristic length that is of the order of the lateral extension of the fluid layer. Being observable only in very shallow liquid layers, the instability usually results in the formation of dry spots.

Another common simplification is the restriction of the instability mechanism to either buoyancy or thermocapillarity [12–14,21], although there seem to be rather few experiments [17,8,11] that have been performed in parameter regions consistent with this assumption. Also, most investigations focused on a single-layer model in which a lower liquid layer is in contact with a gaseous upper layer and only the hydrodynamics of the liquid is treated. The convection in the gas layer is usually neglected and the heat exchange between the layers is often modeled in a phenomenological way using a Biot number; see, e.g., [18]. Even if a genuine two-layer model is considered the viscous stresses and the pressure variations in the gaseous layer are neglected in order to keep the analysis simple [13].

On the other hand, it has been known for some time [12,19] that a system of *two superimposed liquids* displays a much richer behavior than the single-layer models. In particular, the Marangoni instability can be induced by heating from *above*, such that buoyancy and thermocapillarity compete rather than enhance each other, a situation which in single-layer systems can be realized only using the rare case of liquids with anomalous thermocapillary effect in which the surface tension *increases* with increasing temperature [20]. Many additional features such as oscillatory instabilities [14,18] or transitions from up hexagons to down hexagons may be found in systems with two liquid layers. The rich variety of phenomena occurring in the theoretical analysis of two-layer liquid systems results in part from their huge parameter space. A single-layer system is characterized by just three dimensionless parameters; namely, the Rayleigh number, the Marangoni number, and the Prandtl number. The last is irrelevant in a linear analysis and the first two are both proportional to the temperature difference across the layer. Two-layer systems on the other hand may easily need ten or more dimensionless parameters for complete specification. These numbers include the ratios of the hydrodynamic parameters of the participating liquids.

For a long time Marangoni convection in two-liquid-layer systems was an interesting theoretical problem but too difficult to handle experimentally. Zeren and Reynolds have already [12] tried to experimentally realize the instability by heating from above (which came out of their theoretical analysis) but failed. Very recently, however, experiments were performed in which the Marangoni instability in 1–2 mm thick superimposed layers of immiscible liquids was observed [22,23]. In particular, an instability by heating from above and square patterns at onset were reported.

In the present paper we will investigate theoretically Bénard-Marangoni convection in a system of two liquid layers. Building on the linear stability theory developed in [24], we perform a weakly nonlinear analysis in order to solve the planform selection problem slightly above the linear stability threshold. To this end the competition between rolls, squares,

*Email address: andreas.engel@physik.uni-magdeburg.de

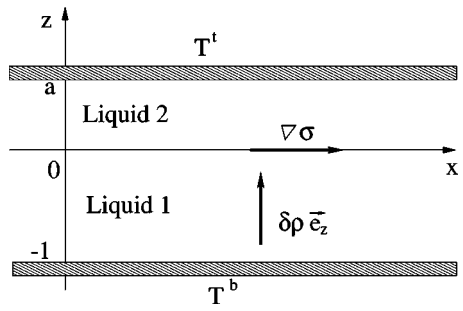

FIG. 1. Sketch of the system under consideration. One liquid layer is superposed on another between two horizontally infinite, perfectly heat conducting plates. The interface between the liquids is assumed to be flat. Convection arises due to buoyancy and the temperature dependence of the surface tension.

and hexagons will be discussed. Only perfect patterns will be considered, leaving the question of weakly modulated patterns for future investigation. We will consistently include buoyancy effects and treat the full hydrodynamics of both liquids, generalizing in this way various previous treatments [6,13,16,25–27]. However, we will assume a flat interface between the two liquids. As will become clear below, interface distortions are crucial for the long wavelength instability resulting in dry spots but can be safely neglected when dealing with the finite wavelength instability resulting in cellular patterns.

The paper is organized as follows. In Sec. II the basic equations are collected and transformed into a form suitable for the weakly nonlinear analysis. Then the perturbation scheme is set up and the necessary computational steps are listed. Section III deals with the first order of perturbation theory, which is nothing but the linear stability analysis. In Sec. IV the main steps of the nonlinear analysis are outlined. The solution of the second-order problem is relegated to Appendix C and the solvability condition in third order is then formulated to derive the desired amplitude equation characterizing the planform selection problem. Section V collects the results obtained for several experimentally relevant combinations of liquids. Finally, Sec. VI contains a discussion of the results together with a comparison with experimental findings.

II. BASIC EQUATIONS

We investigate a system of two layers of immiscible and incompressible liquids of thickness $h^{(i)}$ with densities $\rho^{(i)}$, kinematic viscosities $\nu^{(i)}$, coefficients of volume expansion $\alpha^{(i)}$, heat diffusivities $\chi^{(i)}$, and thermal conductivities $\kappa^{(i)}$ where the superscript $i=1(2)$ denotes the lower (upper) fluid (see Fig. 1). The system is bounded in the vertical direction by two solid, perfectly heat conducting walls with fixed temperatures T^b and T^t and is infinite in the horizontal directions. The interface between the two fluids is assumed to be flat and to lie in the *x-y* plane of the coordinate system.

The hydrodynamics of the two liquids will be described within the Boussinesq approximation, i.e., we assume that all parameters are independent of the temperature, except for the densities $\rho^{(i)}$ and the interface tension σ. More precisely, we use $\rho^{(i)}(T)=\rho^{(i)}(T^b)[1-\alpha^{(i)}(T-T^b)]$ and $\nabla_\perp\sigma=d\sigma/dT\nabla_\perp T$ with constant $\alpha^{(i)}$ and $d\sigma/dT$. Neglecting heat production due to viscosity, the basic equations describing the system are the continuity equations

$$\nabla\cdot\boldsymbol{v}^{(i)}=0, \tag{2.1}$$

the Navier-Stokes equations

$$\partial_t\boldsymbol{v}^{(i)}+(\boldsymbol{v}^{(i)}\cdot\nabla)\boldsymbol{v}^{(i)}=-\frac{1}{\rho^{(i)}}\nabla p^{(i)}-g[1-\alpha^{(i)}(T^{(i)}-T^b)]\boldsymbol{e}_z+\nu^{(i)}\Delta\boldsymbol{v}^{(i)}, \tag{2.2}$$

and the equations of heat conduction

$$\partial_t T^{(i)}+(\boldsymbol{v}^{(i)}\cdot\nabla)T^{(i)}=\chi^{(i)}\Delta T^{(i)}. \tag{2.3}$$

Here $\boldsymbol{e}_z$ denotes the unit vector in the vertical direction and g is the acceleration due to gravity.

The equations are completed by the boundary conditions

$$\boldsymbol{v}^{(1)}=\boldsymbol{0},\quad T^{(1)}=T^b\quad\text{at}\quad z=-h^{(1)} \tag{2.4}$$

and

$$\boldsymbol{v}^{(2)}=\boldsymbol{0},\quad T^{(2)}=T^t\quad\text{at}\quad z=h^{(2)}, \tag{2.5}$$

at the bottom and top, respectively, and

$$\boldsymbol{v}^{(1)}=\boldsymbol{v}^{(2)},\quad T^{(1)}=T^{(2)},\quad \kappa^{(1)}\partial_z T^{(1)}=\kappa^{(2)}\partial_z T^{(2)},$$

$$[(\sigma^{(2)}-\sigma^{(1)})\boldsymbol{e}_z]_\perp=-\frac{d\sigma}{dT}\nabla_\perp T,\quad v_z^{(1)}=v_z^{(2)}=0\quad\text{at}\quad z=0, \tag{2.6}$$

expressing the continuity of the velocities, temperatures, and heat fluxes, respectively as well as the balance of tangential stresses at the interface. The $\sigma^{(i)}$ denote the stress tensors in the liquids and the subscript $\perp$ describes the projection on the *x-y* plane. In accordance with our assumption of a flat interface between the liquids the condition for the continuity of the normal stress at the interface is replaced by the requirement that the perpendicular components of the flow velocities must vanish. This is expressed by the last equation in (2.6).

Introducing $h^{(1)}$, $(h^{(1)})^2/\chi^{(1)}$, $\chi^{(1)}/h^{(1)}$, and $\rho^{(1)}\nu^{(1)}\chi^{(1)}/(h^{(1)})^2$ as units for length, time, velocity, and pressure, respectively, we find for the velocities $\boldsymbol{v}=(u,v,w)$ $[\boldsymbol{V}=(U,V,W)]$ and the appropriately normalized *deviations* θ (Θ) of the temperatures from their static profiles in the lower (upper) liquid the equations

$$\frac{1}{\mathrm{Pr}}[\partial_t\boldsymbol{v}+(\boldsymbol{v}\cdot\nabla)\boldsymbol{v}]=-\nabla\tilde{p}+R\theta\boldsymbol{e}_z+\Delta\boldsymbol{v}, \tag{2.7}$$

$$\partial_t\theta+(\boldsymbol{v}\cdot\nabla)\theta=w+\Delta\theta, \tag{2.8}$$

$$\frac{1}{\mathrm{Pr}}[\partial_t\boldsymbol{V}+(\boldsymbol{V}\cdot\nabla)\boldsymbol{V}]=-\nabla\tilde{P}+\alpha R\Theta\boldsymbol{e}_z+\nu\Delta\boldsymbol{V}, \tag{2.9}$$

$$\partial_t\Theta+(\boldsymbol{V}\cdot\nabla)\Theta=\frac{1}{\kappa}W+\chi\Delta\Theta, \tag{2.10}$$

where the pressure fields $\tilde{p}$ and $\tilde{P}$ in the lower and the upper liquid differ from $p^{(1)}$ and $p^{(2)}$ respectively only by trivial contributions stemming from the buoyancy terms. The boundary conditions acquire the form

$$\boldsymbol{v}=\boldsymbol{0}, \quad \theta=0 \quad \text{at} \quad z=-1, \tag{2.11}$$

$$\boldsymbol{V}=\boldsymbol{0}, \quad \Theta=0 \quad \text{at} \quad z=a, \tag{2.12}$$

and

$$\begin{gathered}\boldsymbol{v}_\perp=\boldsymbol{V}_\perp, \quad w=W=0, \quad \theta=\Theta, \quad \partial_z\theta=\kappa\partial_z\Theta, \\ \partial_z^2 w-\eta\partial_z^2 W=M\Delta_\perp\theta \quad \text{at} \quad z=0,\end{gathered} \tag{2.13}$$

where in the last equation the continuity equation was used. Moreover, the following parameters have been introduced:

$$\begin{gathered}a=\frac{h^{(2)}}{h^{(1)}}, \quad \alpha=\frac{\alpha^{(2)}}{\alpha^{(1)}}, \quad \nu=\frac{\nu^{(2)}}{\nu^{(1)}}, \quad \eta=\nu\frac{\rho^{(2)}}{\rho^{(1)}}, \\ \kappa=\frac{\kappa^{(2)}}{\kappa^{(1)}}, \quad \chi=\frac{\chi^{(2)}}{\chi^{(1)}},\end{gathered} \tag{2.14}$$

as well as the Prandt number $\mathrm{Pr}=\nu^{(1)}/\chi^{(1)}$, the Rayleigh number

$$R=\frac{\alpha^{(1)}g(h^{(1)})^3}{\nu^{(1)}\chi^{(1)}}\frac{\kappa}{a+\kappa}(T^b-T^t), \tag{2.15}$$

and the Marangoni number

$$M=-\frac{d\sigma}{dT}\frac{h^{(1)}}{\nu^{(1)}\rho^{(1)}\chi^{(1)}}\frac{\kappa}{a+\kappa}(T^b-T^t). \tag{2.16}$$

For the Rayleigh and Marangoni numbers we have chosen the standard expressions corresponding to the lower liquid. The numbers for the upper liquid are then given by

$$R^{(2)}=\frac{\alpha a^4}{\nu\chi\kappa}R \quad \text{and} \quad M^{(2)}=\frac{a^2}{\chi\eta\kappa}M, \tag{2.17}$$

respectively.

The ratio between the Rayleigh and Marangoni numbers determines whether the occurring instability is predominantly driven by buoyancy or by surface tension. Experimentally, both parameters are varied simultaneously since they are both proportional to the temperature difference T^b-T^t. We will therefore replace R by cM with the temperature independent constant

$$c=\frac{R}{M}=-\frac{\alpha^{(1)}g\rho^{(1)}(h^{(1)})^2}{d\sigma/dT} \tag{2.18}$$

specifying the experimental setup. In this way both buoyancy and surface tension are included in a consistent way. We assume that $d\sigma/dT<0$ as is the case for most systems of two liquids such that $c>0$. Note that both the situations of heating from below and heating from above are described, with the latter case corresponding to $M<0$.

The set of equations may be simplified by standard manipulations. Taking twice the curl of the Navier-Stokes equations, using the continuity equations, and projecting onto $\boldsymbol{e}_z$, we get the following basic set of equations for the z components of the velocities and the temperature fields:

$$\begin{aligned}\Delta^2 w+cM\Delta_\perp\theta=\frac{1}{\mathrm{Pr}}\{&\partial_t\Delta w-\partial_z[\boldsymbol{\nabla}_\perp\cdot(\boldsymbol{v}\cdot\boldsymbol{\nabla})\boldsymbol{v}_\perp] \\ &+\Delta_\perp(\boldsymbol{v}\cdot\boldsymbol{\nabla})w\},\end{aligned} \tag{2.19}$$

$$w+\Delta\theta=\partial_t\theta+(\boldsymbol{v}\cdot\boldsymbol{\nabla})\theta, \tag{2.20}$$

$$\begin{aligned}\nu\Delta^2 W+\alpha cM\Delta_\perp\Theta=\frac{1}{\mathrm{Pr}}\{&\partial_t\Delta W-\partial_z[\boldsymbol{\nabla}_\perp\cdot(\boldsymbol{V}\cdot\boldsymbol{\nabla})\boldsymbol{V}_\perp] \\ &+\Delta_\perp(\boldsymbol{V}\cdot\boldsymbol{\nabla})W\},\end{aligned} \tag{2.21}$$

$$\frac{1}{\kappa}W+\chi\Delta\Theta=\partial_t\Theta+(\boldsymbol{V}\cdot\boldsymbol{\nabla})\Theta, \tag{2.22}$$

together with the boundary conditions

$$w=\partial_z w=\theta=0 \quad \text{at} \quad z=-1, \tag{2.23}$$

$$\begin{gathered}w=W=0, \partial_z w=\partial_z W, \theta=\Theta, \partial_z\theta=\kappa\partial_z\Theta, \\ \partial_z^2 w-\eta\partial_z^2 W=M\Delta_\perp\theta \quad \text{at} \quad z=0,\end{gathered} \tag{2.24}$$

$$W=\partial_z W=\Theta=0 \quad \text{at} \quad z=a. \tag{2.25}$$

In order to investigate the planform selection problem we will derive third-order amplitude equations for the slow time variation of the amplitudes of different unstable modes. Similar to the case of the Rayleigh-Bénard instability [2], the no-slip boundary conditions at top and bottom suppress the vertical vorticity, i.e., $(\boldsymbol{\nabla}\times\boldsymbol{v})\cdot\boldsymbol{e}_z=(\boldsymbol{\nabla}\times\boldsymbol{V})\cdot\boldsymbol{e}_z=0$, and therefore we do not expect problems due to coupling to a slowly varying mean flow [28] up to this order. From the solution of Eqs. (2.19)–(2.22) we hence obtain w, θ, W, and Θ. Using the continuity equations and the absence of vertical vorticity allows us to determine u, v, and U, V, and finally the pressure fields follow from the Navier-Stokes equations.

It is convenient to write the above equations in the form

$$L\varphi=\mathcal{T}(\varphi)+\mathcal{N}(\varphi,\varphi) \tag{2.26}$$

with the state vector

$$\varphi=\begin{pmatrix} w \\ \theta \\ W \\ \Theta \end{pmatrix}, \tag{2.27}$$

the linear operator L defined by

$$L=\begin{pmatrix} \Delta^2 & cM\Delta_\perp & 0 & 0 \\ 1 & \Delta & 0 & 0 \\ 0 & 0 & \nu\Delta^2 & \alpha cM\Delta_\perp \\ 0 & 0 & 1/\kappa & \chi\Delta \end{pmatrix}, \tag{2.28}$$

and the boundary conditions (2.23)–(2.25). $\mathcal{T}(\varphi)$ denotes the time dependent terms and $\mathcal{N}(\varphi,\varphi)$ describes the quadratic

nonlinearity in Eqs. (2.19)–(2.22). We will solve Eq. (2.26) perturbatively using the *Ansätze*

$$\varphi=\varepsilon\varphi_0+\varepsilon^2\varphi_1+\varepsilon^3\varphi_2+\cdots, \tag{2.29}$$

$$M=M_c+\varepsilon M_1+\varepsilon^2 M_2+\cdots, \tag{2.30}$$

$$\partial_t=i\omega+\varepsilon^2\partial_\tau+\cdots \tag{2.31}$$

with a small parameter ε. In the case of a static instability we have $\omega=0$. For an oscillatory instability $\omega\neq 0$ gives the frequency of oscillation of the unstable mode. Using the perturbation expansion specified above we consider a situation slightly above the threshold M_c of the linear instability, where the amplitude of the unstable modes can still be considered to be small. Putting Eqs. (2.29)–(2.31) into Eq. (2.26), taking into account that Eq. (2.30) implies an expansion

$$L=L_0+\varepsilon L_1+\varepsilon^2 L_2+\cdots \tag{2.32}$$

for the linear operator, and matching powers of ε, the nonlinear problem transforms into a sequence of linear equations of the form

$$L_0\varphi_0=0, \tag{2.33}$$

$$L_0\varphi_1=-L_1\varphi_0+\mathcal{N}(\varphi_0,\varphi_0), \tag{2.34}$$

$$L_0\varphi_2=-L_2\varphi_0-L_1\varphi_1+\mathcal{T}(\varphi_0)+\mathcal{N}(\varphi_1,\varphi_0)+\mathcal{N}(\varphi_0,\varphi_1). \tag{2.35}$$

The first line is just the linear stability problem. The condition for nontrivial solutions φ_0 of this equation makes L_0 singular and yields the critical value M_c of the bifurcation parameter M. From the translation invariance in the x-y plane we know that φ_0 is of the form

$$\varphi_0=\varphi_0(z)\exp(i\boldsymbol{k}\cdot\boldsymbol{r}-i\omega t), \tag{2.36}$$

where $\boldsymbol{r}=(x,y)$ and $\boldsymbol{k}=(k_x,k_y)$ are two-dimensional vectors. There is a critical value $M_c(k)$ of the bifurcation parameter for all values of $|\boldsymbol{k}|=k$ and minimizing $M_c(k)$ in k gives the wave number k_c of the first unstable mode together with the critical Marangoni number $M_c=M_c(k_c)$.

The remaining equations in the hierarchy starting with Eq. (2.34) all involve the *very same* singular operator L_0 but are *inhomogeneous*. Consequently, the perturbation expansion makes sense only if the inhomogeneities are perpendicular to the zero eigenfunction of the adjoint operator L_0^+ of L_0.

In order to address the planform selection problem within the perturbation approach sketched above the form of φ_0 must be sufficiently general and in particular must include the different planforms observed in experiment. We will discuss the planform selection problem only for the case of the static instability, leaving the investigation of the oscillatory instability to future work. It is then sufficient to use for φ_0 the form

$$\varphi_0=\varphi_0(z)\left[\sum_{n=1}^{6}A_n(\tau)e^{i\boldsymbol{k}_n\cdot\boldsymbol{r}}+\text{c.c.}\right] \tag{2.37}$$

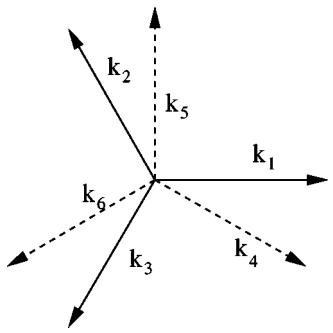

FIG. 2. Relative orientation of the two-dimensional wave vectors appearing in the *Ansatz* (2.37). The two triads $\boldsymbol{k}_1,\boldsymbol{k}_2,\boldsymbol{k}_3$ and $\boldsymbol{k}_4,\boldsymbol{k}_5,\boldsymbol{k}_6$ of wave vectors with $\boldsymbol{k}_5$ perpendicular to $\boldsymbol{k}_1$ allow us to describe rolls as well as squares and hexagons by different values for the amplitudes A_n in Eq. (2.37).

with the six two-dimensional vectors $\boldsymbol{k}_n$ obeying $|\boldsymbol{k}_n|=k_c$ and $\boldsymbol{k}_1+\boldsymbol{k}_2+\boldsymbol{k}_3=\boldsymbol{0}$, $\boldsymbol{k}_4+\boldsymbol{k}_5+\boldsymbol{k}_6=\boldsymbol{0}$, as well as $\boldsymbol{k}_1\cdot\boldsymbol{k}_5=0$ (see Fig. 2). Depending on the values of the amplitudes A_n, this form describes rolls (e.g., $A_1=A$, $A_n=0$ for all $n>1$), squares (e.g., $A_1=A_5=A$, $A_n=0$ else), and hexagons (e.g., $A_1=A_2=A_3=A$, $A_n=0$ for $n>3$).

Using this form we find from the solvability conditions of Eqs. (2.34) and (2.35) an equation describing the time evolution of the scaled amplitudes $\tilde{A}_n=\varepsilon A_n$. As is well known [2] the *general* form of this amplitude equation already follows from the symmetries of the problem. For the present situation it is given by

$$\partial_t\tilde{A}_1=\epsilon\tilde{A}_1+\gamma\tilde{A}_2^*\tilde{A}_3^*-[|\tilde{A}_1|^2+g_h(|\tilde{A}_2|^2+|\tilde{A}_3|^2)+g_t(|\tilde{A}_4|^2+|\tilde{A}_6|^2)+g_n|\tilde{A}_5|^2]\tilde{A}_1 \tag{2.38}$$

with the supercriticality parameter

$$\epsilon=\frac{M-M_c}{M_c}. \tag{2.39}$$

Similar equations for the other amplitudes follow from permutation and complex conjugation. The terms included in these equations are the only ones up to third order that are invariant under the transformation $A_n\mapsto A_n\exp(i\boldsymbol{k}_n\cdot\boldsymbol{r}_0)$ corresponding to a translation by $\boldsymbol{r}_0$ in the x-y plane. Moreover, due to the isotropy in the x-y plane the coupling coefficients between the different terms in Eq. (2.37) may only depend on the angle between the corresponding wave vectors.

The amplitude equation (2.38) is of potential type and can be written in the form

$$\partial_t\tilde{A}_i=-\frac{\partial F(\tilde{A}_1,\ldots\tilde{A}_6^*)}{\partial\tilde{A}_i^*}. \tag{2.40}$$

A well known linear stability analysis of the various fixed points of Eq. (2.38) corresponding to the extrema of F yields the stability regions of the different planforms as functions of the parameters $\epsilon,\gamma,g_h,g_t,g_n$ [29]. The remaining problem is thus to use the perturbation expansion described above to express these coefficients of the amplitude equation in terms

of the hydrodynamic parameters of the problem. To this end the following well-known program has to be carried through.

(1) Calculate $M_c(k)$ from the linear problem and determine $k_c = \mathrm{argmin} M_c(k)$ and $M_c = M_c(k_c)$.

(2) Determine the adjoint operator L_0^+ of L_0 and its zero eigenfunction $\overline{\varphi_0}$.

(3) Calculate the inhomogeneity of the $O(\varepsilon^2)$ equation (2.34) and apply the solvability condition to this order.

(4) Solve the $O(\varepsilon^2)$ equation (2.34) to determine φ_1.

(5) Calculate the inhomogeneity of the $O(\varepsilon^3)$ equation (2.35) [only terms proportional to $\exp i(\boldsymbol{k}_1 \cdot \boldsymbol{r})$ are necessary].

(6) Combine the solvability conditions at order $O(\varepsilon^2)$ and $O(\varepsilon^3)$ to derive Eq. (2.38) and extract the expressions for the parameters γ, g_h, g_t, g_n.

III. LINEAR PROBLEM

We first solve the $O(\varepsilon)$ problem (2.33), which is equivalent to the linear stability analysis. Putting $\varphi_0 = \varphi_0(z)\exp(i\boldsymbol{k}\cdot\boldsymbol{r} - i\omega t)$ and using the *Ansätze*

$$w_0(z), \theta_0(z) \sim \exp(\lambda z), \quad W_0(z), \Theta_0(z) \sim \exp(\Lambda z), \tag{3.1}$$

we find

$$(\lambda^2 - k_c^2)\left(\lambda^2 - k_c^2 + \frac{i\omega}{\mathrm{Pr}}\right)(\lambda^2 - k_c^2 + i\omega) = -cMk_c^2,$$

$$(\Lambda^2 - k_c^2)\left(\Lambda^2 - k_c^2 + \frac{i\omega}{\nu \mathrm{Pr}}\right)\left(\Lambda^2 - k_c^2 \frac{i\omega}{\chi}\right) = -\frac{\alpha}{\nu\kappa\chi} cMk_c^2. \tag{3.2}$$

We therefore obtain six different values for λ_i and Λ_i. It is convenient to define $\lambda_i = \Lambda_{i-6}$ for $i = 7,...,12$ and to write

$$w_0(z) = \sum_{i=1}^{6} w_{0i} e^{\lambda_i z}, \quad \theta_0(z) = -\sum_{i=1}^{6} \frac{w_{0i}}{\lambda_i^2 - k_c^2 + i\omega} e^{\lambda_i z}, \tag{3.3}$$

$$W_0(z) = \sum_{i=7}^{12} w_{0i} e^{\lambda_i z},$$

$$\Theta_0(z) = -\frac{1}{\kappa\chi} \sum_{i=7}^{12} \frac{w_{0i}}{\lambda_i^2 - k_c^2 + i\omega/\chi} e^{\lambda_i z}. \tag{3.4}$$

The boundary conditions (2.23)–(2.25) then give rise to a homogeneous system of linear equations for the 12 unknowns w_{0i}. In order to get a nontrivial solution the determinant of the coefficient matrix $\mathcal{A}$ must vanish. The conditions for the real and imaginary parts of $\det \mathcal{A}$ yield the desired functions $M_c(k;\mathrm{par})$ and $\omega_c(k,\mathrm{par})$ where $\mathrm{par} = (a, \alpha, \kappa, \chi, \nu, \eta, c, \mathrm{Pr})$ stands for the vector of parameters in the problem.

A typical result for a static instability is shown in Fig. 3 displaying the dispersion curve resulting from the numerical analysis of $\det \mathcal{A} = 0$ for $\omega = 0$ using the parameters of setup 5 listed in Appendix A. As can be seen from the figure, in this system one may have an instability by heating from below ($M > 0$) as well as when heating from above ($M < 0$). When comparing the dispersion relations with those resulting from the full linear stability analysis including surface deflections as considered in [24], one finds that in the region of the pattern-forming instability $k \cong 1-3.5$ the two curves are indistinguishable in a plot like Fig. 3. Differences show up only for small wave numbers $k \ll 1$. Within the linear theory surface deflections for short wavelength modes involved in the planform selection problem may therefore safely be neglected. We expect that this holds true also in the weakly nonlinear regime.

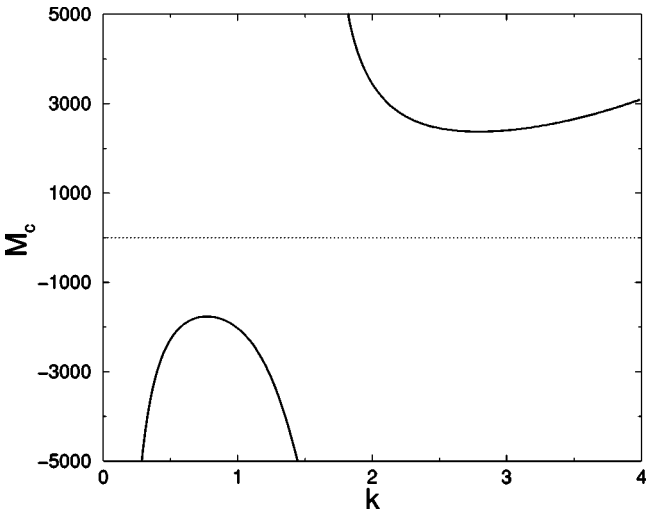

FIG. 3. Dispersion relation $M_c(k)$ as resulting from the linear stability analysis for the hydrodynamic parameters of setup 5 listed in Appendix A. The system shows an instability when heated from below ($M > 0$) as well as one when heated from above ($M < 0$).

Having obtained the dispersion relation we calculate k_c by minimizing $M_c(k)$ and determine the critical Marangoni and Rayleigh numbers of both fluids as well as the temperature difference across both layers at the instability. The results for the setups under consideration are summarized in the upper part of Table I in Sec. V below.

Of all the parameters of the system the depth ratio a is the only one that may easily be varied in experiments. For the parameters of setup 9 and a total depth of 4.5 mm we have calculated the critical Marangoni number and the critical wave number modulus as a function of the thickness $h^{(1)}$ of the bottom layer, restricting ourselves to the case of heating from below but including the possibility of an oscillatory instability. The results are displayed in Fig. 4. For values of $h^{(1)}$ between 1.5 and 2.5 an oscillatory instability precedes the static one, which would occur at unusually large Marangoni numbers only. A similar oscillatory instability was also found for a two-layer system in which the Marangoni effect was neglected and pure buoyancy-driven convection was considered, and an intuitive interpretation as a periodic change between viscous and thermal coupling of the flow fields at the interface was given [14].

Knowing the critical value of M we can now also determine the coefficients of the eigenvector corresponding to the zero eigenvalue. This fixes the functions $w_0(z)$, $\theta_0(z)$, $W_0(z)$, and $\Theta_0(z)$ up to an overall constant and completes the determination of φ_0.

Finally, we have to consider the adjoint problem and to

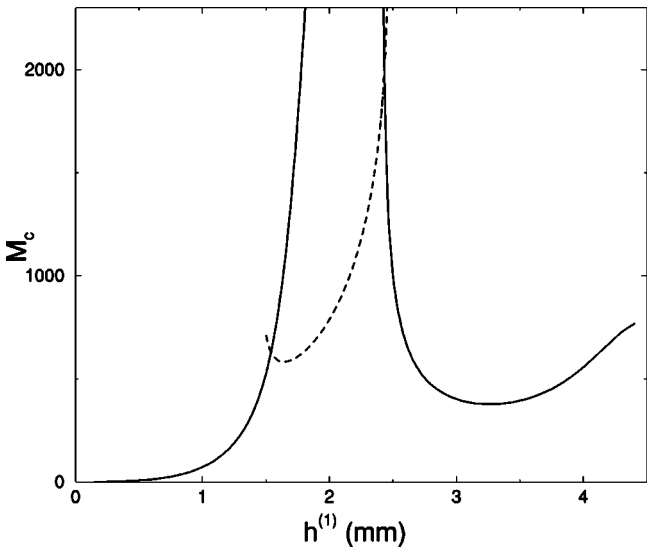

FIG. 4. Critical Marangoni number for a static (full line) and oscillatory (dashed line) instability when heating from below a system with parameters as specified in setup 9 of Appendix A and total depth 4.5 mm, as a function of the bottom layer thickness $h^{(1)}$. Note that both M and k are scaled with $h^{(1)}$ [cf. Eqs. (2.14) and (2.16)].

calculate its zero eigenfunction $\overline{\varphi_0}$ where we again restrict ourselves to the stationary instability. The adjoint operator L^+ is determined in Appendix B. The calculation of its eigenfunction to the eigenvalue zero is very similar to the determination of φ_0 described above. We find that it is of the form $\overline{\varphi_0}\exp(i\boldsymbol{k}_n\cdot\boldsymbol{r})$ where the components of $\overline{\varphi_0}$ may be written as

$$\overline{w}_0(z)=\sum_{i=1}^{6}\overline{w}_{0i}e^{\lambda_i z},\quad \overline{\theta}_0(z)=cMk_c^2\sum_{i=1}^{6}\frac{\overline{w}_{0i}}{\lambda_i^2-k_c^2}e^{\lambda_i z}, \tag{3.5}$$

$$\overline{W}_0(z)=\sum_{i=7}^{12}\overline{w}_{0i}e^{\lambda_i z},\quad \overline{\Theta}_0(z)=\frac{\alpha cMk_c^2}{\chi}\sum_{i=7}^{12}\frac{\overline{w}_{0i}}{\lambda_i^2-k_c^2}e^{\lambda_i z} \tag{3.6}$$

with the same parameters λ_i as determined by Eq. (3.2) with $\omega=0$. The boundary conditions again give rise to a 12×12 system of linear homogeneous equations for the coefficients $\overline{\omega}_{0i}$. As before the condition for a nontrivial solution is a vanishing determinant of the corresponding matrix. Note, however, that there is now no parameter to adjust. The deviation of the smallest eigenvalue of the matrix found in the numerical calculation from zero therefore gives a valuable hint of the accuracy of the numerical procedure employed.

IV. NONLINEAR ANALYSIS

The solution of the planform selection problem requires treatment of the nonlinear interaction between different unstable modes. We restrict the nonlinear analysis to the case of a static bifurcation. To include nonlinear terms up to the third order in the amplitudes A_n introduced in Eq. (2.37) we have first to solve Eq. (2.34). The general procedure is standard; some intermediate steps are sketched in Appendix C. Using this solution we are in the position to calculate the terms appearing on the right hand side of Eq. (2.35). We do not have to solve this equation, but only need to know the solvability condition at this order. Due to the x-y integrals in Eq. (B9) and the $\boldsymbol{r}$ dependence of $\overline{\varphi_0}$, only terms proportional to $\exp(\pm i\boldsymbol{k}_n\cdot\boldsymbol{r})$ give rise to nontrivial contributions to the solvability condition. In fact, it is sufficient to focus on terms proportional to $\exp(i\boldsymbol{k}_1\cdot\boldsymbol{r})$ since these finally give rise to an amplitude equation of the form (2.38) for A_1. Equivalent equations for the other amplitudes of the *Ansatz* (2.37) then follow from permutation and complex conjugation.

In order to collect the relevant terms we first realize that there are contributions

$$A_1e^{i\boldsymbol{k}_1\cdot\boldsymbol{r}}\begin{pmatrix} cM_2k_c^2\theta_0\\ 0\\ \alpha cM_2k_c^2\Theta_0\\ 0\\ -M_2k_c^2\theta_0|_{z=0}\end{pmatrix},$$

$$A_2^*A_3^*e^{i\boldsymbol{k}_1\cdot\boldsymbol{r}}\begin{pmatrix} cM_1k_c^2\theta_1\\ 0\\ \alpha cM_1k_c^2\Theta_1\\ 0\\ -M_1k_c^2\theta_1|_{z=0}\end{pmatrix},$$

$$\partial_\tau A_1e^{i\boldsymbol{k}_1\cdot\boldsymbol{r}}\begin{pmatrix} \frac{1}{\mathrm{Pr}}(w_0''-k_c^2w_0)\\ \theta_0\\ \frac{1}{\mathrm{Pr}}(W_0''-k_c^2W_0)\\ \Theta_0\\ 0\end{pmatrix} \tag{4.1}$$

originating from the terms $-L_2\varphi_0$, $-L_1\varphi_1$, and $\mathcal{T}(\varphi_0)$, respectively, in Eq. (2.35). Here θ_1 and Θ_1 denote the solutions obtained in Appendix C for the resonant term.

The contributions proportional to $\exp(i\boldsymbol{k}_1\cdot\boldsymbol{r})$ from the last two terms in Eq. (2.35) arise from combinations between $\varphi_0\sim\exp(i\boldsymbol{q}\cdot\boldsymbol{r})$ and $\varphi_1\sim\exp(i\boldsymbol{p}\cdot\boldsymbol{r})$ with $\boldsymbol{q}+\boldsymbol{p}=\boldsymbol{k}_1$. From the continuity equation $\boldsymbol{\nabla}\cdot\boldsymbol{v}=0$ and the absence of vertical vorticity $(\boldsymbol{\nabla}\times\boldsymbol{v})\cdot\boldsymbol{e}_z=0$, we find

$$\boldsymbol{v}_{0\perp}=e^{i\boldsymbol{q}\cdot\boldsymbol{r}}\frac{i\boldsymbol{q}}{\boldsymbol{q}^2}\partial_z w_0,\quad \boldsymbol{v}_{1\perp}=e^{i\boldsymbol{p}\cdot\boldsymbol{r}}\frac{i\boldsymbol{p}}{\boldsymbol{p}^2}\partial_z w_1, \tag{4.2}$$

which gives rise to

$$\begin{aligned}
&-\partial_z[\boldsymbol{\nabla}_\perp\cdot(\boldsymbol{v}_0\cdot\boldsymbol{\nabla})\boldsymbol{v}_{1\perp}]+\Delta_\perp(\boldsymbol{v}_0\cdot\boldsymbol{\nabla})w_1-\partial_z[\boldsymbol{\nabla}_\perp\cdot(\boldsymbol{v}_1\cdot\boldsymbol{\nabla})\boldsymbol{v}_{0\perp}]\\
&\quad+\Delta_\perp(\boldsymbol{v}_\perp\cdot\boldsymbol{\nabla})w_0\\
&=e^{i\boldsymbol{k}_1\cdot\boldsymbol{r}}\left[\frac{\boldsymbol{k}_1\cdot\boldsymbol{q}}{\boldsymbol{q}^2}w_0'''w_1+\left(\frac{\boldsymbol{k}_1\cdot\boldsymbol{q}}{\boldsymbol{q}^2}-\frac{\boldsymbol{q}\cdot\boldsymbol{p}}{\boldsymbol{q}^2\boldsymbol{p}^2}k_c^2\right)w_0''w_1'\right.\\
&\quad+\left(\frac{\boldsymbol{k}_1\cdot\boldsymbol{p}}{\boldsymbol{p}^2}-\frac{\boldsymbol{q}\cdot\boldsymbol{p}}{\boldsymbol{q}^2\boldsymbol{p}^2}k_c^2\right)w_0'w_1''+\frac{\boldsymbol{k}_1\cdot\boldsymbol{p}}{\boldsymbol{p}^2}w_0w_1'''\\
&\quad\left.+k_c^2\left\{\left(\frac{\boldsymbol{q}\cdot\boldsymbol{p}}{\boldsymbol{q}^2}-1\right)w_0'w_1+\left(\frac{\boldsymbol{q}\cdot\boldsymbol{p}}{\boldsymbol{p}^2}-1\right)w_0w_1'\right\}\right]
\end{aligned} \tag{4.3}$$

TABLE I. Results for the critical temperature difference ΔT over both liquids ($\Delta T>0$ for heating from below, $\Delta T<0$ for heating from above), the critical wave number k_c, the Marangoni and Rayleigh numbers of both liquids at onset, the parameters of the amplitude equation (2.38), the subcritical threshold ϵ_{sub} for the hexagon pattern, its amplitude A_h at onset, the values ϵ_s at which squares become stable and ϵ_h at which hexagons become unstable, and the Maxwell value ϵ_{hms} at which the potential (2.40) is the same for the square and hexagon patterns for setups 1–8 as specified in Appendix A.

	Setup							
Results	1	2	3	4	5	6	7	8
ΔT_c	0.749	1.030	0.485	−1.474	2.901	−1.241	1.469	0.989
k_c	2.481	2.048	2.352	0.692	2.790	0.572	2.395	2.380
M	779	685	647	−872	2370	−450	1352	848
R	726	182	761	−137	530	−42	623	710
$M^{(2)}$	182	183	81	−416	692	−424	205	170
$R^{(2)}$	171	20	20	−277	401	−330	62	56
γ	0.340	0.494	0.340	−0.543	0.4203	−0.579	0.494	0.433
g_h	1.212	1.275	1.232	1.386	1.194	1.353	1.173	1.182
g_t	1.351	1.324	1.418	1.4436	1.467	1.323	1.110	1.149
g_n	0.417	−0.383	0.443	−0.039	0.2379	−0.612	−0.693	−0.4159
ϵ_{sub}	−0.008	−0.017	−0.008	−0.020	−0.013	−0.023	−0.018	−0.014
A_h	0.100	0.139	0.098	0.144	0.124	0.156	0.148	0.129
ϵ_s	0.125	0.038	0.114	0.081	0.108	0.024	0.0192	0.036
ϵ_h	3.850	0.334	6.892	0.984	12.05	0.240	0.112	0.161
ϵ_{hms}	0.277	0.074	0.281	0.162	0.272	0.050	0.036	0.060

and

$$(\boldsymbol{v}_0\cdot\boldsymbol{\nabla})\theta_1+(\boldsymbol{v}_1\cdot\boldsymbol{\nabla})\theta_0 = e^{i\boldsymbol{k}_1\cdot\boldsymbol{r}}\left[\frac{\boldsymbol{q}\cdot\boldsymbol{p}}{\boldsymbol{q}^2}w_0'\theta_1-\frac{\boldsymbol{q}\cdot\boldsymbol{p}}{\boldsymbol{p}^2}w_1'\theta_0+w_0\theta_1'+w_1\theta_0'\right].$$

With the help of these relations it is now easy to determine the remaining terms proportional to $\exp(i\boldsymbol{k}_1\cdot\boldsymbol{r})$ from all the possible combinations for $\boldsymbol{q}$ and $\boldsymbol{p}$ and the corresponding results for φ_1 calculated in Appendix C.

Using the scalar product (B9) and the result for $\overline{\varphi_0}$, the solvability condition at order $O(\varepsilon^3)$ can be formulated. It contains a term proportional to $M_1A_2^*A_3^*$ which, by eliminating M_1 using the solvability condition (C11) at order $O(\varepsilon^2)$, is transformed into terms proportional to $|A_2|^2A_1$ and $|A_3|^2A_1$. We then multiply the solvability condition at order $O(\varepsilon^2)$ by ε^2 and the one at order $O(\varepsilon^3)$ by ε^3 and add them together. Observing that $\varepsilon M_1+\varepsilon^2M_2=M-M_c$, returning to the original time by using $\varepsilon^2\partial_\tau=\partial_t$, and introducing the scaled amplitudes $\tilde{A}_n=\varepsilon A_n$, we eventually end up with an amplitude equation of the form (2.38) with explicit expressions for the parameters γ, g_h, g_t, and g_n.

V. RESULTS

The expressions for γ, g_h, g_t, and g_n are rather long and will not be displayed. Moreover, due to the large number of parameters in the two-liquid system it is more appropriate to analyze some experimentally relevant parameter combinations rather than to display cross sections along various directions of the parameter space. For the experimental setups 1–8 specified in Appendix A the results of the nonlinear analysis are summarized in the middle part of Table I.

In order to finally address the planform selection problem we first note that squares are consistently described by a third-order amplitude equation only if $1+g_n>0$. Otherwise, the third-order term is not saturating and higher orders have to be included, which appears to be quite involved. Consequently the present approach can describe only square patterns bifurcating *supercritically* from the basic state.

Similarly, one must have $1+2g_h>0$ in order to have the hexagon pattern stabilized by the third-order term. Unlike the square and roll patterns, however, hexagons appear *subcritically* at $\epsilon_{\rm sub}=-\gamma^2/4(1+2g_h)$. The small amplitude solution is always unstable.

A detailed linear stability analysis of the roll, square, and hexagon solutions of the amplitude equation (2.38) reveals the following [29,16]. Rolls are stable if $g_h>1$, $g_t>1$, $g_n>1$, and $\epsilon>\epsilon_r=\gamma^2/(1-g_h)^2$. Squares are stable if $1+g_n<g_h+g_t$, $g_n<1$, and $\epsilon>\epsilon_s=\gamma^2(1+g_n)/(1+g_n-g_h-g_t)^2$. Hexagons are stable for all $\epsilon>\epsilon_{sub}$ if $g_h<1$ and $1+2g_h<g_n+2g_t$. If $g_h>1$ they become unstable for $\epsilon>\gamma^2(2+g_h)/(1-g_h)^2$; if $1+2g_h>g_n+2g_t$ this happens for $\epsilon>\gamma^2(g_n+2g_t)/(1+2g_h-g_n-2g_t)^2$. The value of ϵ at which hexagons lose their stability will be denoted by ϵ_h. As is seen from these conditions, squares and rolls are mutually exclusive whereas hexagons may coexist with either squares or rolls. To locate the transition between patterns that are both locally stable the Maxwell value of ϵ at which the potential F defined in Eq. (2.40) has the same value for the two planforms under consideration is of interest [30]. For the setups considered in this paper only the Maxwell value for the transition between hexagons and squares is relevant, which we denote by ϵ_{hms}. The special values of ϵ defined above together with the amplitude A_h of the hexagon pattern at onset for setups 1–8 are collected in the lower part of Table I.

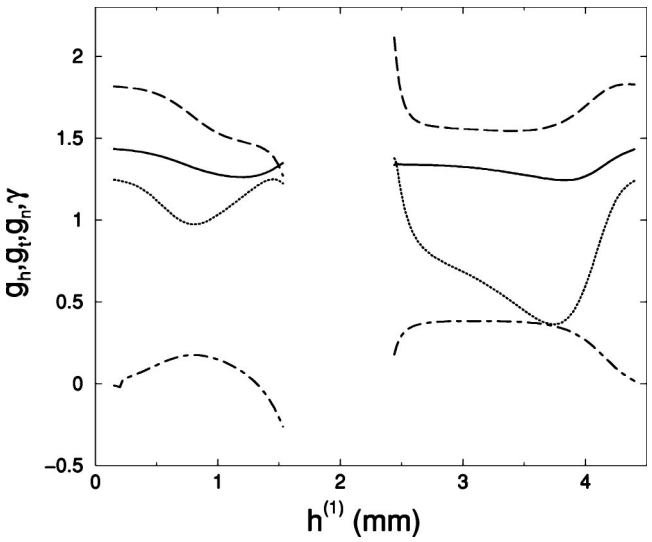

FIG. 5. The parameters g_h (full), g_t (dashed), g_n (dotted) and γ (dashed-dotted) of the amplitude equation (2.38) as functions of the thickness $h^{(1)}$ of the bottom layer for setup 9 with a total layer depth of 4.5 mm and heating from below. For $1.5\,\mathrm{mm} \lesssim h^{(1)} \lesssim 2.5\,\mathrm{mm}$ the oscillatory instability precedes the static one.

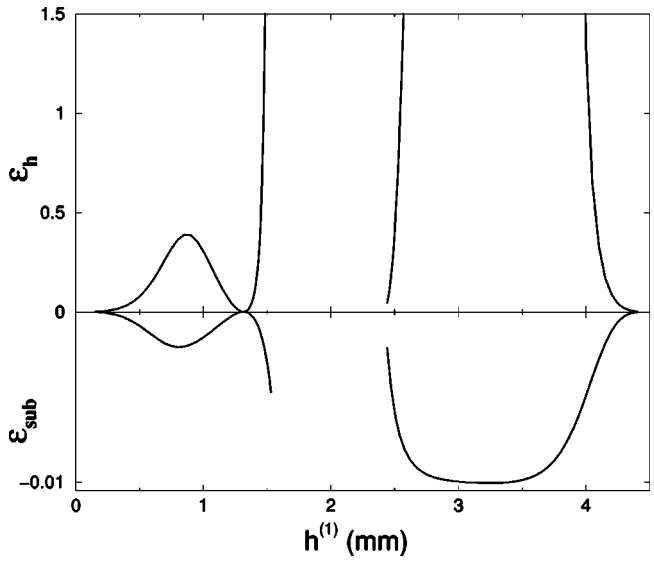

FIG. 6. The values of ϵ_h at which hexagons become unstable and ϵ_{sub} at which hexagons appear subcritically as functions of the thickness $h^{(1)}$ of the bottom layer for setup 9 with a total layer depth of 4.5 mm and heating from below. Note the different scales for positive and negative values at the vertical axis. For $1.5\,\mathrm{mm} \lesssim h^{(1)} \lesssim 2.5\,\mathrm{mm}$ the oscillatory instability precedes the static one.

For the parameters of setup 9 and a total depth of 4.5 mm we have again scanned the dependence of the results of the nonlinear analysis on the thickness of the bottom layer for the case of heating from below. Figure 5 shows the coefficients of the amplitude equation (2.38) as functions of $h^{(1)}$. The most apparent feature is the strong sensitivity of the coefficients to variations of the depth ratio. In experiments the depth must therefore be controlled very accurately in order to allow sensible comparison with the theory. The system under consideration shows a transition from up to down hexagons when varying the depth ratio, as can be seen from the change of sign of γ.

Finally in Fig. 6 the dependence of ϵ_h and ϵ_{sub} on $h^{(1)}$ is displayed. Again a strong sensitivity to the depth ratio is observed. Note that since they are the result of a perturbation expansion in ϵ values of ϵ_h substantially larger than 1 are not reliable.

VI. DISCUSSION

In the present paper a weakly nonlinear analysis for Bénard-Marangoni convection in systems of two superimposed liquids has been developed. A consistent treatment of the full hydrodynamics and heat conduction in both layers was performed. As a crucial simplifying ingredient of our approach we have used the assumption of an undisturbed interface between the liquids. Comparison with the complete linear stability analysis including interface deflections reveals that this approximation is extremely good for a pattern-forming instability occurring at not too long wavelengths. We have considered the planform selection problem by determining the relative stabilities of roll, square, and hexagon patterns. To this end the coefficients of an appropriate amplitude equation were calculated as functions of the hydrodynamic parameters by a perturbation theory in the amplitude of the unstable mode. Explicit results have been obtained for nine specific setups that have recently been investigated experimentally. Since the system is, on the one hand, characterized by nine dimensionless parameters whereas it is, on the other hand, very hard to find two really immiscible fluids to perform the experiments, this seems to be the most sensible way to theoretically investigate the peculiarities of a system that may also be seen in experiments.

For all setups considered we found $1+2g_h>0$, which implies that for hexagons the cubic term is able to stabilize the linear instability. The hexagon pattern occurs subcritically at $\epsilon_{sub}<0$. Strictly speaking, a backward bifurcation leading to a finite amplitude immediately at onset invalidates our perturbation *Ansatz* (2.29) [31]. However, the size of the subcritical region as well as the amplitude of the hexagon pattern at onset were found to be rather small for all setups investigated. This is in accordance with experiment in which it is usually impossible to see the subcritical hysteresis at all [23]. Hence, with the amplitude of the pattern at onset being small, our perturbation *Ansatz* should still be a good approximation for what really happens and the results obtained should be rather accurate.

For all setups we found $g_h>1$ and $1+2g_h>g_n+2g_t$, implying that the hexagon pattern does not remain stable for arbitrarily large ϵ. The value ϵ_h at which hexagons become unstable as obtained within our perturbative analysis is reliable only if it is not too large. Common experience suggests that the values are trustworthy if they are smaller than 1.

Another general result for all setups studied is that $g_n<1$, excluding rolls as stable planforms at threshold. We find for all setups $\epsilon_s<\epsilon_h$, indicating that hexagons and squares coexist for a given interval of ϵ. The general situation is hence as shown for setup 7 in Fig. 7.

All values for ϵ_h and ϵ_s found are *strictly positive*, implying that exactly at onset our analysis always predicts hexagons as the only stable planform. This is in accordance with what was found experimentally for setups 1–6. For setups 7 and 8 squares at onset were seen in the experiment. These

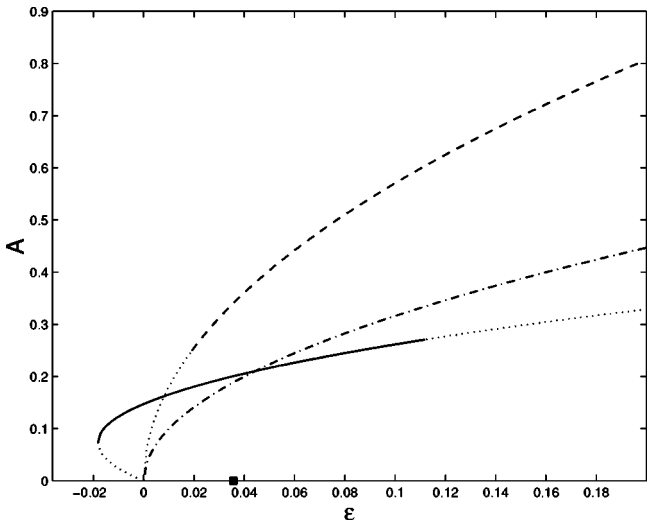

FIG. 7. Amplitudes of the hexagon (full line), square (dashed line), and roll (dash-dotted) patterns as functions of the criticality parameter ϵ for the planform selection problem corresponding to setup 7 as specified in Appendix A. The dotted parts of the curves denote unstable solutions; the roll pattern is always unstable. The square on the ϵ axis gives the value ϵ_{hms} for which the hexagon and square planforms realize the same value of the potential F defined in Eq. (2.40).

setups are characterized by rather small values of ϵ_h and extremely small values of ϵ_s. Note in this connection that in [32] the transition from hexagons to squares in an experiment with a single fluid layer was reported to occur at $\epsilon \cong 4.2$ with the theoretical value resulting from a numerical integration of the Navier-Stokes equation being even higher. For setups 7 and 8 we would hence predict theoretically that immediately above onset squares become stable and that for somewhat larger ϵ the hexagon pattern loses stability. It is then quite conceivable to observe experimentally a mixture of squares and hexagons immediately at onset. Note that our theoretical analysis treats only perfect patterns, hardly occurring in the experiment, and that due to boundaries and impurities a nucleation of square patches may set in well before ϵ_h is reached. This is also plausible from the small values of the Maxwell value ϵ_{hms}. Altogether, we therefore claim that our results for setups 7 and 8 are in good agreement with the experimental finding of squares at onset. For both setups a secondary transition from squares to rolls was found experimentally, which we fail to reproduce theoretically. The reason for this discrepancy may be that the transition occurs outside the validity of our perturbation approach.

The detailed comparison between our theoretical and the corresponding experimental results for the other setups is as follows. For setup 1 a hexagon pattern is found experimentally at $\epsilon \cong 0.28$ [Fig. 7(a) in [23]], consistent with the theory, which finds both hexagons and squares stable for this value of ϵ. In setup 2 a mixture of hexagons and squares is found at $\epsilon \cong 1.72$ [Fig. 7(b) in [23]], whereas the theory excludes hexagons and predicts squares as the only stable planform. This difference may be related to the rather large value of ϵ. For setup 3 the experiment finds hexagons for $0 < \epsilon < 0.27$ (Fig. 8 in [23]), again consistent with theory, which predicts squares to be only metastable for $\epsilon < \epsilon_{hms} \cong 0.28$. The same holds true for setup 5 [Fig. 12(b) in [23]], in which the experiment gives hexagons at $\epsilon \cong 0.136$ and theory predicts squares to be metastable up to $\epsilon \cong 0.27$. For the two setups with heating from above, namely, setups 4 and 6 [Figs. 12(a) and 13, respectively, in [23]], the experimentally found hexagon planform is at variance with theory. At the relevant values $\epsilon \cong 1.56$ and $\epsilon \cong 1.8$, respectively, hexagons should already be unstable. Again the discrepancy between theory and experiment occurs for rather large ϵ. Also, patterns with heating from above were very difficult to obtain experimentally and the values of ϵ given for the experiments may not be very accurate [33].

For setup 9 the dependence of the several parameters determining the planform on the depth ratio was the main focus of the investigation. As shown in Figs. 5 and 6 the parameters of the amplitude equation and the special values of ϵ resulting from them may depend very sensitively on the depth ratio. Since the latter cannot be controlled with arbitrary precision in experiments, comparison with theory always needs some care. As for setups 7 and 8, one finds for setup 9 that for some $h^{(1)}$ the values of ϵ_h can be so small (cf. Fig. 6) that it is again easily conceivable to miss the hexagonal pattern completely in the experiment and to observe squares as the first pattern after the instability in accordance with the experimental findings. Note in this connection that together with ϵ_h the absolute value of ϵ_{sub} characterizing the subcritical stability region of the hexagon planform also gets very small, such that hexagons exist only in an extremely small window around criticality.

The oscillatory instability found for setup 9 was also detected in the experiment [23] for $h^{(1)} \cong 1.8$ mm, in accordance with Fig. 4. The experimental values for the critical Marangoni number and the wavelength and frequency of the oscillatory mode are in satisfactory agreement with the linear theory as already discussed in [23].

The sign of γ is related to the detailed convection pattern of the hexagon planform. For $\gamma > 0$ the hexagons in the lower fluid are up hexagons (liquid rises in the center) and the ones in the upper layer are down hexagons. For $\gamma < 0$ the situation is reversed. We do not know of experimental results concerning this feature for the two-liquid Marangoni problem.

The remaining discrepancies between theoretical and experimental findings might be due to the perturbative character of our derivation. In particular, there is the possibility of so-called asymmetric squares in pattern-forming hydrodynamic systems [34], which, bifurcating *discontinuously* from the quiescent state, do not show up in a perturbative approach.[1] At the moment it is not clear whether these patterns can already be expected at the small values of the parameter ϵ used in the experiments. Since the flow pattern of asymmetric squares is rather different from that of conventional squares it might be possible to clarify experimentally which form of squares has been observed.

ACKNOWLEDGMENTS

We have very much benefited from discussions with Anne Juel and Harry Swinney. A.E. would also like to thank F.

[1] We would like to thank F. Busse for pointing out this possibility to us.

TABLE II. Substances, depths, and interface tensions for the nine setups analyzed in this paper. For the characterization of the liquids used see Table III below.

	Bottom layer		Top layer			
Setup	Substance	Depth (mm)	Substance	Depth (mm)	$d\sigma/dT$ (N/mK)	Heating from
1	HT 135	1.91	silicon oil 5cS	2.69	-7.3×10^{-5}	below
2	HT 135	1.02	silicon oil 2cS	0.87	-7.3×10^{-5}	below
3	HT 135	2.14	silicon oil 5cS	2.21	-7.3×10^{-5}	below
4	HT 70	0.80	silicon oil 5cS	2.26	-7.3×10^{-5}	above
5	HT 70	0.95	silicon oil 5cS	2.11	-7.3×10^{-5}	below
6	HT 70	0.61	silicon oil 5cS	2.45	-7.3×10^{-5}	above
7	HT 70	1.02	water	2.22	-4.1×10^{-5}	below
8	FC 75	1.28	water	2.78	-4.73×10^{-5}	below
9	Acetonitrile	$h^{(1)}$	*n*-hexane	$4.5-h^{(1)}$	-1×10^{-4}	below

Busse, S. W. Morris, and W. Pesch for interesting discussions and Jean Bragard and Wayne Tokaruk for very useful correspondence. Part of the work was done during a visit by A.E. at the Center for Nonlinear Dynamics at the University of Texas at Austin. He would like to thank all members of the Center for their kind hospitality and the Volkswagenstiftung for financial support. The work of J.B.S. was supported by the NASA Office of Life and and Microgravity Sciences Grant No. NAG3-1839.

APPENDIX A: PARAMETER VALUES

This Appendix provides the values of the hydrodynamic parameters used in the explicit calculations of the present paper (Table II). All nine setups correspond to experimentally relevant combinations. Experiments with setups 1–7 are discussed in [23]; setup 8 was used in the experiments reported in [22]. The dependence of the instability and the planform on the depth ratio was experimentally studied by Juel [33] using setup 9. Note that the value of $d\sigma/dT$ is difficult to determine experimentally; the values given are therefore rough estimates or fitted from the linear analysis.

Table III contains the hydrodynamic parameters for the different liquids used. More details are to be found in the original experimental papers [23] and [22].

APPENDIX B: OPERATOR EXPANSION AND ADJOINT PROBLEM

The decomposition (2.32) of the linear operator is not completely straightforward for the Marangoni problem because the bifurcation parameter M occurs not only in the linear operator but also in the corresponding boundary conditions. A transparent way to deal with the situation is to include the boundary condition involving M into the operator L [7], which is then written in the form

$$L=\begin{pmatrix} \Delta^2 & cM\Delta_\perp & 0 & 0 & 0 \\ 1 & \Delta & 0 & 0 & 0 \\ 0 & 0 & \nu\Delta^2 & \alpha cM\Delta_\perp & 0 \\ 0 & 0 & 1/\kappa & \chi\Delta & 0 \\ \partial_z^2|_{z=0} & 0 & -\eta\partial_z^2|_{z=0} & 0 & -M\Delta_\perp \end{pmatrix}, \tag{B1}$$

acting now on the correspondingly augmented state vector

$$\varphi=\begin{pmatrix} w \\ \theta \\ W \\ \Theta \\ \theta|_{z=0} \end{pmatrix}. \tag{B2}$$

The operator is completed by the boundary conditions

$$w=\partial_z w=\theta=0 \quad \text{at} \quad z=-1, \tag{B3}$$

TABLE III. Hydrodynamic parameters for the different liquids investigated.

Substrate	ρ (kg/m^3)	ν (10^{-6} m^2/s)	κ (J/ms K)	c_p (J/kg K)	α (10^{-8} K)
HT 70	1680	0.5	0.07	962	1.10
HT 135	1730	1.0	0.07	962	1.10
Silicon oil 5cS	920	5.0	0.117	1590	1.05
Silicon oil 2cS	873	2.0	0.109	1713	1.17
FC 75	1760	0.945	0.0635	1046	1.40
Water	998	1.0	0.60	4182	0.207
Acetonitrile	776	0.476	0.188	2230	1.41
n-hexane	655	0.458	0.120	2270	1.41

$$w=W=0, \quad \partial_z w=\partial_z W, \quad \theta=\Theta, \quad \partial_x\theta=\kappa\partial_z\Theta \quad \text{at} \quad z=0, \tag{B4}$$

$$W=\partial_z W=\Theta=0 \quad \text{at} \quad z=a, \tag{B5}$$

which differ from Eqs. (2.23)–(2.25) just by the omission of the boundary condition involving M. We now easily find

$$L_0=\begin{pmatrix} \Delta^2 & cM_c\Delta_\perp & 0 & 0 & 0 \\ 1 & \Delta & 0 & 0 & 0 \\ 0 & 0 & \nu\Delta^2 & \alpha c M_c\Delta_\perp & 0 \\ 0 & 0 & 1/\kappa & \chi\Delta & 0 \\ \partial_z^2|_{z=0} & 0 & -\eta\partial_z^2|_{z=0} & 0 & -M_c\Delta_\perp \end{pmatrix}, \tag{B6}$$

$$L_1=\begin{pmatrix} 0 & cM_1\Delta_\perp & 0 & 0 & 0 \\ 0 & 0 & 0 & 0 & 0 \\ 0 & 0 & 0 & \alpha c M_1\Delta_\perp & 0 \\ 0 & 0 & 0 & 0 & 0 \\ 0 & 0 & 0 & 0 & -M_1\Delta_\perp \end{pmatrix}, \tag{B7}$$

and

$$L_2=\begin{pmatrix} 0 & cM_2\Delta_\perp & 0 & 0 & 0 \\ 0 & 0 & 0 & 0 & 0 \\ 0 & 0 & 0 & \alpha c M_2\Delta_\perp & 0 \\ 0 & 0 & 0 & 0 & 0 \\ 0 & 0 & 0 & 0 & -M_2\Delta_\perp \end{pmatrix}, \tag{B8}$$

where all three operators are completed by the boundary conditions (B3)–(B5).

The adjoint operator is defined by $\langle\overline{\varphi}|L\varphi\rangle=\langle L^+\overline{\varphi}|\varphi\rangle$. Introducing the scalar product

$$\langle\overline{\varphi}|\varphi\rangle=\lim_{L\to\infty}\frac{1}{L^2}\int_{-L/2}^{L/2}dx\int_{-L/2}^{L/2}dy\left[\int_{-1}^{0}dz(\overline{w}^*w+\overline{\theta}^*\theta)+\int_0^a dz(\overline{W}^*W+\overline{\Theta}^*\Theta)+\partial_z\overline{w}^*|_{z=0}\theta|_{z=0}\right], \tag{B9}$$

we find after some partial integration that L^+ is given by

$$L^+=\begin{pmatrix} \Delta^2 & 1 & 0 & 0 & 0 \\ cM\Delta_\perp & \Delta & 0 & 0 & 0 \\ 0 & 0 & \nu\Delta^2 & 1/\kappa & 0 \\ 0 & 0 & \alpha c M\Delta_\perp & \chi\Delta & 0 \\ 0 & -\partial_z|_{z=0} & 0 & \chi\partial_z|_{z=0} & -M\Delta_\perp \end{pmatrix} \tag{B10}$$

acting on the augmented vector

$$\overline{\varphi}=\begin{pmatrix} \overline{w} \\ \overline{\theta} \\ \overline{W} \\ \overline{\Theta} \\ \partial_z\overline{w}|_{z=0} \end{pmatrix} \tag{B11}$$

and completed by the boundary conditions

$$\overline{w}=\partial_z\overline{w}=\overline{\theta}=0 \quad \text{at} \quad z=-1, \tag{B12}$$

$$\overline{w}=\overline{W}=0, \quad \partial_z\overline{w}=\frac{1}{\rho}\partial_z\overline{W}, \quad \partial_z^2\overline{w}=\nu\partial_z^2\overline{W},$$

$$\overline{\theta}=\frac{\chi}{\kappa}\overline{\Theta} \quad \text{at} \quad z=0, \tag{B13}$$

$$\overline{W}=\partial_z\overline{W}=\overline{\Theta}=0 \quad \text{at} \quad z=a. \tag{B14}$$

It is, of course, possible to transform back the last line of L^+ into a boundary condition and this is indeed advantageous to determine $\overline{\varphi}_0$ explicitly; however, for use in the solvability conditions the above augmented form is the most appropriate one.

APPENDIX C: THE $O(\varepsilon^2)$ PROBLEM

In this appendix we solve Eq. (2.34) for the case of a static instability. From the term $\mathcal{N}(\varphi_0,\varphi_0)$ and the structure (2.37) of φ_0 it is clear that the right hand side of this equation will contain several terms with different exponential factors of the form $\exp[i(\pm\boldsymbol{k}_n\pm\boldsymbol{k}_m)\cdot\boldsymbol{r}]$. Because of the linearity of the equation we may solve it separately for all these terms in the inhomogeneity.

Let us start with the so-called *nonresonant* terms in which the angle ϕ between $\pm\boldsymbol{k}_n$ and $\pm\boldsymbol{k}_m$ is different from $2\pi/3$. It is clear then from the *x, y* integrals in Eq. (B9) that for these terms $\langle\overline{\varphi_0}|\mathcal{N}(\varphi_0,\varphi_0)\rangle=0$. In view of Eq. (B7) the solvability condition boils down to $M_1=0$ and hence removes the $L_1\varphi_0$ term from the inhomogeneity of Eq. (2.34). Using the form (2.37) of φ_0 we therefore find as equations for φ_1

$$\Delta^2 w_1+cM_c\Delta_\perp\theta_1=A_nA_m e^{i(\pm\boldsymbol{k}_n\pm\boldsymbol{k}_m)\cdot\boldsymbol{r}}\frac{2}{\mathrm{Pr}}([1+\cos(\phi)]\times\{w_0'''w_0+[1-2\cos(\phi)]w_0'w_0''\}-2k_c^2\sin^2(\phi)w_0w_0'),$$

$$w_1+\Delta\theta_1=A_nA_m e^{i(\pm\boldsymbol{k}_n\pm\boldsymbol{k}_m)\cdot\boldsymbol{r}}2[w_0\theta_0'-\cos(\phi)w_0'\theta_0],$$

$$\nu\Delta^2 W_1+\alpha cM\Delta_\perp\Theta_1=A_nA_m e^{i(\pm\boldsymbol{k}_n\pm\boldsymbol{k}_m)\cdot\boldsymbol{r}}\frac{2}{\mathrm{Pr}}([1+\cos(\phi)]\times\{W_0'''W_0+[1-2\cos(\phi)]W_0'W_0''\}-2k_c^2\sin^2(\phi)W_0W_0'),$$

$$\frac{1}{\kappa}W_1+\chi\Delta\Theta_1=A_nA_m e^{i(\pm\boldsymbol{k}_n\pm\boldsymbol{k}_m)\cdot\boldsymbol{r}}2[W_0\Theta_0'-\cos(\phi)W_0'\Theta_0],$$

where the prime denotes differentiation with respect to *z*. Since $M_1=0$ the boundary conditions completing this set of equations are given by Eqs. (2.23)–(2.25) with $M=M_c$.

The solution of these equations is of the form $\varphi_1=A_nA_m\varphi_1(z)\exp[i(\pm\boldsymbol{k}_n\pm\boldsymbol{k}_m)\cdot\boldsymbol{r}]$. We first determine a solution of the inhomogeneous equations using the *Ansätze*

$$w_1^{inh}(z)=\sum_{i,j=1}^{6}w_{1ij}e^{(\lambda_i+\lambda_j)z},\quad \theta_1^{inh}(z)=\sum_{i,j=1}^{6}\theta_{1ij}e^{(\lambda_i+\lambda_j)z},\tag{C1}$$

$$W_1^{inh}(z)=\sum_{i,j=7}^{12}w_{1ij}e^{(\lambda_i+\lambda_j)z},\quad \Theta_1^{inh}(z)=\sum_{i,j=7}^{12}\theta_{1ij}e^{(\lambda_i+\lambda_j)z},\tag{C2}$$

which give rise to algebraic equations for the coefficients w_{1ij}, θ_{1ij}, W_{1ij}, and Θ_{1ij} in terms of w_{0i} and λ_i. This solution does not yet satisfy the boundary conditions. We therefore add an appropriate solution of the homogeneous equation, which is written in the form

$$w_1^{hom}(z)=\sum_{i=1}^{6}w_{1i}^{hom}e^{\tilde{\lambda}_i z},$$

$$\theta_1^{hom}(z)=-\sum_{i=1}^{6}\frac{w_{1i}^{hom}}{\tilde{\lambda}_i^2-2k_c^2[1+\cos(\phi)]}e^{\tilde{\lambda}_i z},\tag{C3}$$

$$W_1^{hom}(z)=\sum_{i=7}^{12}w_{1i}^{hom}e^{\tilde{\lambda}_i z},$$

$$\Theta_1^{hom}(z)=-\frac{1}{\kappa\chi}\sum_{i=7}^{12}\frac{w_{1i}^{hom}}{\tilde{\lambda}_i^2-2k_c^2[1+\cos(\phi)]}e^{\tilde{\lambda}_i z},\tag{C4}$$

with $\tilde{\lambda}_i$ satisfying

$$\{\tilde{\lambda}_i^2-2k_c^2[1+\cos(\phi)]\}^3=\begin{cases}-2cM_ck_c^2[1+\cos(\phi)] & \text{for } i=1,\ldots,6\\ -2\dfrac{\alpha}{\kappa\nu\chi}cM_ck_c^2[1+\cos(\phi)] & \text{for } i=7,\ldots,12.\end{cases}\tag{C5}$$

Note that $\tilde{\lambda}_i\neq\lambda_i$. Therefore the determinant of the matrix in the inhomogeneous set of linear equations for w_{1i}^{hom} is different from zero and the solution is unique. Note also that for $\phi=\pi$ the procedure can be simplified since $w_1(z)=W_1(z)=0$.

As for the *resonant* terms arising from the interaction of modes with an angle $\phi=2\pi/3$ between their respective $\pm\boldsymbol{k}$ vectors, let us focus on the one proportional to $\exp(i\boldsymbol{k}_1\cdot\boldsymbol{r})$. It is has one contribution proportional to A_1 stemming from $-L_1\varphi_0$ and another one proportional to $A_2^*A_3^*$ originating from $\mathcal{N}(\varphi_0,\varphi_0)$ in Eq. (2.34). Using L_1 as defined by Eq. (B7), the resulting equations are of the form

$$\Delta^2 w_1+cM_c\Delta_\perp\theta_1=e^{i\boldsymbol{k}_1\cdot\boldsymbol{r}}\frac{A_2^*A_3^*}{\mathrm{Pr}}(w_0'''w_0+2w_0'w_0''-3k_c^2w_0w_0')+A_1cM_1k_c^2\theta_0,\tag{C6}$$

$$w_1+\Delta\theta_1=e^{i\boldsymbol{k}_1\cdot\boldsymbol{r}}A_2^*A_3^*(2w_0\theta_0'+w_0'\theta_0),\tag{C7}$$

$$\nu\Delta^2 W_1+\alpha cM\Delta_\perp\Theta_1=e^{i\boldsymbol{k}_1\cdot\boldsymbol{r}}\frac{A_2^*A_3^*}{\mathrm{Pr}}(W_0'''W_0+2W_0'W_0''-3k_c^2W_0W_0')+A_1\alpha cM_1k_c^2\Theta_0,\tag{C8}$$

$$\frac{1}{\kappa}W_1+\chi\Delta\Theta_1=e^{i\boldsymbol{k}_1\cdot\boldsymbol{r}}A_2^*A_3^*(2W_0\Theta_0'+W_0'\Theta_0).\tag{C9}$$

The boundary conditions are again given by Eqs. (2.23)–(2.25) except for the one containing the Marangoni number, which is modified to [cf. Eq. (B7)]

$$\partial_z^2 w_1 - \eta \partial_z^2 W_1 - M_c \Delta_\perp \theta_1 = -A_1 e^{i\mathbf{k}_1\cdot\mathbf{r}} M_1 k_c^2 \theta_0 \quad \text{at} \quad z=0. \tag{C10}$$

Due to the resonant factor $e^{i\mathbf{k}_1\cdot\mathbf{r}}$ the terms arising from $\mathcal{N}(\varphi_0,\varphi_0)$ are not automatically perpendicular to $\overline{\varphi_0}$, and using Eq. (B9) the solvability condition acquires the nontrivial form

$$\begin{aligned}0 = A_2^* A_3^* \Bigg[& \int_{-1}^{0} dz \Bigg(\frac{\overline{w_0}^*}{\mathrm{Pr}} (w_0''' w_0 + 2 w_0' w_0'' - 3 k_c^2 w_0 w_0') \\ & + \overline{\theta_0}^* (2 w_0 \theta_0' + w_0' \theta_0) \Bigg) + \int_0^a dz \Bigg(\frac{\overline{W_0}^*}{\mathrm{Pr}} (W_0''' W_0 + 2 W_0' W_0'' \\ & - 3 k_c^2 W_0 W_0') + \overline{\Theta}_0^* (2 W_0 \Theta_0' + W_0' \Theta_0) \Bigg) \Bigg] \\ & + A_1 c M_1 k_c^2 \Bigg[\int_{-1}^{0} dz \overline{w_0}^* \theta_0 + \alpha \int_0^a dz \overline{W_0}^* \Theta_0 \\ & - \frac{1}{c} \partial_z \overline{w_0}^*|_{z=0} \theta_0|_{z=0} \Bigg].\end{aligned} \tag{C11}$$

We use this equation to replace the terms involving M_1 in Eqs. (C6)–(C9) and in the boundary condition (C10). The solutions to these equations can then be written in the form $A_2^* A_3^* \varphi_1(z) e^{i\mathbf{k}_1\cdot\mathbf{r}}$. Again, we first determine a particular solution of the inhomogeneous equations by using the *Ansätze*

$$w_1^{inh}(z) = \sum_{i,j=1}^{6} w_{1ij} e^{(\lambda_i+\lambda_j)z} + \sum_{i=1}^{6} w_{1i} z e^{\lambda_i z},$$

$$\theta_1^{inh}(z) = \sum_{i,j=1}^{6} \theta_{1ij} e^{(\lambda_i+\lambda_j)z} + \sum_{i=1}^{6} (\theta_{1i} z + \tilde{\theta}_{1i}) e^{\lambda_i z},$$

$$W_1^{inh}(z) = \sum_{i,j=7}^{12} w_{1ij} e^{(\lambda_i+\lambda_j)z} + \sum_{i=7}^{12} w_{1i} z e^{\lambda_i z},$$

$$\Theta_1^{inh}(z) = \sum_{i,j=7}^{12} \theta_{1ij} e^{(\lambda_i+\lambda_j)z} + \sum_{i=7}^{12} (\theta_{1i} z + \tilde{\theta}_{1i}) e^{\lambda_i z}.$$

To satisfy the boundary conditions we add a solution of the homogeneous equations which must be of the form [cf. Eqs. (3.3), (3.4)]

$$w_1^{hom}(z) = \sum_{i=1}^{6} w_{1i}^{hom} e^{\lambda_i z}, \quad \theta_1^{hom}(z) = -\sum_{i=1}^{6} \frac{w_{1i}^{hom}}{\lambda_i^2 - k_c^2} e^{\lambda_i z}, \tag{C12}$$

$$W_1^{hom}(z) = \sum_{i=7}^{12} w_{1i}^{hom} e^{\lambda_i z},$$

$$\Theta_1^{hom}(z) = -\frac{1}{\kappa\chi} \sum_{i=7}^{12} \frac{w_{1i}^{hom}}{\lambda_i^2 - k_c^2} e^{\lambda_i z}. \tag{C13}$$

The boundary conditions give rise to an *inhomogeneous* system of linear equations for the coefficients w_{1i}^{hom} with the same singular matrix $\mathcal{A}$ that appeared in the linear stability analysis. Due to the solvability condition (C11), however, the inhomogeneity of this set of linear equations is perpendicular to the zero eigenvector of the adjoint problem and therefore the system admits solutions. Their numerical determination is most conveniently done by using the singular value decomposition of the matrix $\mathcal{A}$ [35]. This method yields an approximate solution even if the solvability condition is not fulfilled exactly, which will always be the case due to numerical errors. Moreover, the so-called residual quantifying the deviation from the exactly solvable case gives another check on the numerical accuracy of the whole procedure.

Finally, the solution for w_{1i}^{hom} obtained in this way is not unique since one can always add a solution of the homogeneous equations. We will enforce the additional constraint

$$\begin{aligned}0 = (\varphi_0|\varphi_1) := \lim_{L\to\infty} \frac{1}{L^2} \int_{-L/2}^{L/2} dx \int_{-L/2}^{L/2} dy \Bigg[& \int_{-1}^{0} dz (w_0^* w_1 \\ & + \theta_0^* \theta_1) + \int_0^a dz (W_0^* W_1 + \Theta_0^* \Theta_1) \Bigg]\end{aligned} \tag{C14}$$

to remove this ambiguity. The rationale behind this requirement is as follows. Assume that we knew the exact solution φ of the full nonlinear problem. According to Eqs. (2.29) and (2.37) we want A_n to be the amplitude of the contribution to φ proportional to $\exp(i\mathbf{k}_n\cdot\mathbf{r})$, i.e., $(\exp(i\mathbf{k}_n\cdot\mathbf{r})\varphi_0(z)|\varphi) = \varepsilon A_n$. Using the expansion (2.39) for φ, this results in $(\varphi_0|\varphi_l) = 0$ for all $l \geq 1$. Note the use of different scalar products in Eqs. (C14) and (B9).

This completes the solution of the $O(\varepsilon^2)$ equations. The results are specified by the various matrices w_{1ij}, w_{1i}, w_{1i}^{hom}, θ_{1ij}, θ_{1i}, $\tilde{\theta}_{1i}$, and θ_{1i}^{hom}.

[1] H. Bénard, Rev. Gen. Sci. Pures Appl. **11**, 1261 (1900).
[2] M. C. Cross and P. C. Hohenberg, Rev. Mod. Phys. **65**, 851 (1993).
[3] Lord Rayleigh, Philos. Mag. **32**, 529 (1916).
[4] M. J. Block, Nature (London) **178**, 650 (1956).
[5] J. R. A. Pearson, J. Fluid Mech. **4**, 489 (1958).
[6] J. Scanlon and L. Segel, J. Fluid Mech. **30**, 149 (1967).
[7] A. Cloot and G. Lebon, J. Fluid Mech. **145**, 447 (1984).
[8] M. F. Schatz, S. J. VanHook, W. D. McCormick, J. B. Swift, and H. L. Swinney, Phys. Rev. Lett. **75**, 1938 (1995).
[9] L. E. Scriven and C. V. Sternling, J. Fluid Mech. **19**, 321 (1964).
[10] K. A. Smith, J. Fluid Mech. **24**, 401 (1966).
[11] S. J. VanHook, M. F. Schatz, W. D. McCormick, J. B. Swift, and H. L. Swinney, Phys. Rev. Lett. **75**, 4397 (1995); J. Fluid Mech. **345**, 45 (1997).
[12] R. W. Zeren and W. C. Reynolds, J. Fluid Mech. **53**, 305 (1972).
[13] A. A. Golovin, A. A. Nepomnyashchy, and L. M. Pismen, J. Fluid Mech. **341**, 317 (1997).
[14] S. Rasenat, F. H. Busse, and I. Rehberg, J. Fluid Mech. **199**, 519 (1989).

[15] E. L. Koschmieder and M. I. Biggerstaff, J. Fluid Mech. **167**, 49 (1986).
[16] J. Bragard and M. G. Velarde, J. Fluid Mech. **368**, 165 (1998).
[17] I. B. Simanovskii and A. A. Nepomnyashchy, *Convective Instabilities in Systems with Interface* (Gordon and Breach, Amsterdam, 1993).
[18] L. M. Bravermann, K. Eckert, A. A. Nepomnyashchy, I. B. Simanovskii, and A. Thess, report (unpublished).
[19] An oscillatory instability can also be found in a one-layer model with surface deflection when heating from below [15,16]. The magnitude of the critical Marangoni number is, however, very large.
[20] M. Takashima, J. Phys. Soc. Jpn. **50**, 2751 (1981).
[21] C. Perez-Garcia and G. Carneiro, Phys. Fluids A **3**, 292 (1991).
[22] W. A. Tokaruk, T. C. A. Molteno, and S. W. Morris, Phys. Rev. Lett. **84**, 3590 (2000).
[23] A. Juel, J. M. Burgess, W. D. McCormick, J. B. Swift, and H. L. Swinney, Physica D (to be published).
[24] S. VanHook, J. Small, and J. B. Swift (unpublished).
[25] J. Bragard and G. Lebon, Europhys. Lett. **21**, 831 (1993).
[26] M. Bestehorn, Phys. Rev. Lett. **76**, 46 (1996).
[27] P. M. Parmentier, V. C. Regnier, G. Lebon, and J. C. Legros, Phys. Rev. E **54**, 411 (1996).
[28] E. D. Siggia and A. Zippelius, Phys. Rev. Lett. **47**, 835 (1981).
[29] S. Ciliberto, P. Coullet, J. Lega, E. Pampaloni, and C. Perez-Garcia, Phys. Rev. Lett. **65**, 2370 (1990).
[30] E. Bodenschatz, J. R. de Bruyn, G. Ahlers, and D. S. Cannell, Phys. Rev. Lett. **67**, 3078 (1991).
[31] F. H. Busse, J. Fluid Mech. **30**, 625 (1967).
[32] K. Eckert, M. Bestehorn, and A. Thess, J. Fluid Mech. **356**, 155 (1998).
[33] A. Juel (private communication).
[34] F. H. Busse and R. M. Clever, Phys. Rev. Lett. **81**, 341 (1998).
[35] W. H. Press, B. P. Flannery, S. A. Teukolsky, and W. T. Vetterling, *Numerical Recipes in C* (Cambridge University Press, Cambridge, England, 1990).